Applied Surface Science 462 (2018) 669–677

Contents lists available at ScienceDirect

Applied Surface Science

journal homepage: www.elsevier.com/locate/apsusc

Full Length Article

Ion excitation and etching effects on top-surface properties of sp^2 nanocrystallited carbon films

Xue Fan, Dongfeng Diao*

Institute of Nanosurface Science and Engineering, Guangdong Provincial Key Laboratory of Micro/Nano Optomechatronics Engineering, Shenzhen University, Shenzhen 518060, China

ARTICLE INFO

Keywords:
Ion excitation
Ion etching
Sp^2 nanocrystallited carbon film
Top-surface properties

ABSTRACT

We proposed the low energy ion irradiation effects (ion excitation and ion etching) on the formation and the top-surface properties of sp^2 nanocrystallited carbon films in electron cyclotron resonance (ECR) plasma sputtering system. In this work, the ion etching rate during film deposition was measured and a threshold voltage for physical etching was found to be about 35 V. Below the threshold voltage, the film growth was induced by ion excitation effect (ion exciting electrons of top-most atoms), as a result, the sp^2 dominant nanocrystallite size in the films was large. When the ion energy exceeded the threshold voltage, the film growth was induced by ion etching effect (ion breaking covalent bond), and the nanocrystallite size was small confirmed by the transmission electron microscopy (TEM) observation and Raman analysis. Furthermore, the top-surface properties of sp^2 nanocrystallite carbon films prepared with different ion irradiation effects were examined by using the atomic force microscopy (AFM). Results showed that the ion etched carbon films had smaller surface roughness, scratch depth and adhesive force compared with the ion excited carbon films. These findings shed light on the fabrication and applications of carbon based nanostructured materials.

1. Introduction

Carbon films with sp^2 nanocrystallite embedded in have attracted extensive studies due to the integrated properties such as excellent mechanical [1], electrical [2], magnetical [3] and photovoltaic [4] properties. For tailoring the nanostructure of carbon films, electron or ion irradiation are both effective methods [5–9]. For example, sp^2-bonded nanocrystallites have been formed in the carbon films with relatively high temperature and moderate ion irradiation energy [8], and graphene nanocrystallites embedded in carbon films can be formed with low-energy electron excitation effect in an electron cyclotron resonance plasma [9]. However, the electron irradiated carbon films were usually soft with rough surface [10]. It has been reviewed that ion irradiation can lead to self-organization or self-assembly in nanostructures of carbon systems [11]. When irradiation effects in carbon are considered, the contributions can be divided into those that lead to a displacement of atoms and those that do not. Generally, with increasing particle energy excitations decrease in importance, whereas displacement of atoms effects increase [12]. Therefore, during the ion irradiation, the threshold energy, which is the minimum energy required to irreversibly displace a carbon atom, is a fundamental parameter to control the nanostructure of carbon films [13]. When the ion irradiation energy is larger than the threshold energy, increasing dangling bond densities at the exposed growth surface can be formed [14]. In the electron cyclotron resonance (ECR) plasma sputtering, ion irradiation can be realized through applying negative substrate bias under divergent magnetic field, and the ion irradiation energy can be adjusted by changing the substrate bias voltage easily [15,16]. However, well-defined nanostructure of carbon films fabricated with low energy ion irradiation effects still needs to be developed.

As for a nanoscale protective layer, the top-surfaces are of critical importance in determining the performance of nanodevices. In order to avoid the surface nanocontact, ultrasmooth surfaces are usually needed. Ion irradiation is an intriguing tool for topography engineering of surfaces at nanometer length scale [17,18]. Films with arithmetic mean roughness as low as 0.1 nm was achieved by flattening the surface locally where the energy of the incident ions is dissipated [19]. For the demand of superhard protective nanosurface, tetrahedron carbon films with high sp^3 bonding component as much as possible [20], or nanocrystallite carbon film with highly tangled cross-linked structure between graphite basal planes [21] were developed. With the high energy ion irradiation, cross-linking between graphene basal planes can be formed by external inducement [22,23], which can be expected to result in an excellent mechanical properties of carbon films. The surface

* Corresponding author.
E-mail address: dfdiao@szu.edu.cn (D. Diao).

https://doi.org/10.1016/j.apsusc.2018.08.148
Received 13 November 2017; Received in revised form 31 July 2018; Accepted 18 August 2018
Available online 20 August 2018
0169-4332/

adhesion is also an important property that needs to be considered, since it has been studied that surface adhesion can induce nano-response in terms of re-indentation at nanoscale [24], and adhesion between two material surfaces will prevent the relative movement converting the mechanical energy to electricity in the tribotronic devices [25]. The surface adhesion can be affected not only by the surface roughness [26], but also by the other factors such as surface energy, surface termination, and the nanostructure [27,28]. For the nanostructured carbon films, the effect of embedded nanocrystallite on the surface adhesion is an open question. Therefore, as mentioned above, the top-surface properties of nanocrystallited carbon films with different ion irradiation effects needs to be clarified.

In this paper, low energy ion irradiation in ECR plasma sputtering was used for fabricating sp^2 dominant nanocrystallited carbon films. The ion irradiation effects were studied by the threshold voltage for physical etching, which was obtained by the ion etching rate during film deposition. The nanostructures of carbon films with different ion irradiation effects were observed and analyzed by high-resolution electron transmission microscopy (TEM), electron energy-loss spectroscopy (EELS), X-Ray photoelectron spectroscopy (XPS) and Raman spectra. The top-surface properties, which including the surface roughness, surface nanoscratch and surface adhesion were studied by atomic force microscopy (AFM) with its different functions. Finally, the ion irradiation effects on the nanostructure and the top-surface properties were verified by the carbon films with after growth ion irradiation.

2. Experiments

2.1. Low energy ion irradiation

The low energy ion irradiation was conducted in electron cyclotron resonance (ECR) plasma. Divergent magnetic field was formed with magnetic coil working on the target side. A cylindrical carbon target was placed in the filming chamber, and the magnetic coil current was adjusted to make the ECR point (magnetic flux equals to 875 G) just nearby the target to increase the sputtering rate. A p-type Si ⟨1 0 0⟩ substrate (thickness, 500 μm; size, 20 mm × 20 mm) was used, which was set 17 cm far away from the ECR point. The schematic of ECR system layout was shown in Fig. 1(a). The chamber was pumped to a background pressure of 4.0×10^{-4} Pa with mechanical and molecular pumps. Pure argon was employed as the working gas and the gas pressure was maintained at 6×10^{-2} Pa. The argon gas was charged with 2.45 GHz microwave power (500 W) at the ECR point. In this plasma generation condition, the plasma density ranged from 12×10^{10} cm^3 at the ECR point to 1.0×10^{10} cm^3 at the substrate surface, the ion current density to the substrate was 5.8 mA/cm^2 and the substrate floating voltage was −12 V. The schematic for film growth with ion irradiation is shown in Fig. 1(b). A glassy carbon target is used as solid carbon source. DC bias voltage of −500 V was applied on the carbon target, and the target current was 0.9 A during deposition. Substrate bias voltage from 0 to −88 V was chosen to fabricate carbon films, and the ions were accelerated to the substrate by the folded electronic fields with floating voltage and substrate bias voltage. Therefore, the ion irradiation energy was interpreted by the ion accelerating voltage (V_{ion}), which was changed from 12 V to 100 V. The film thickness was controlled to be 40 nm with film growth rate ranging from 8 to 10 nm/min according to different ion accelerating voltages. For the ECR plasma sputtering system, the Ar plasma energy distribution is more focusing, and the higher end of the energy profile, which sometimes sputters carbon ions, is shorter [29]. Therefore, the most of the sputtered particles are carbon atoms or molecules, and the irradiation effects by carbon ions can be neglected during film deposition. Also, the standout feature of ECR plasma sputtering is that the plasma can be generated only by applying microwave and magnetic field to the ion source without applying voltage to the carbon target. So that, the pure ion irradiation method achieves the same ion irradiation conditions as those for film formation process. Therefore, in order to examine the ion irradiation effect, we performed after growth ion irradiation, that is pure argon ion irradiating on the as-deposited carbon film with V_{ion} of 12 V, as shown in Fig. 1(c). The ion accelerating voltages for after growth ion irradiation were 12 V, 20 V, 35 V, 40 V, 50 V, 60 V, 75 V, 90 V and 100 V. The irradiation processes lasted for 10 min to test the irradiation depth. No substrate heating was performed during and after the film growth, and the substrate temperature was below 50 °C shown from a temperature indicator.

2.2. Nanostructure characterization

High-resolution transmission electron microscopy (TEM) was used to observe the nanostructures and perform the electron energy-loss spectroscopy (EELS). TEM specimens for cross-sectional view observation were prepared by rough mechanical thinning and precise ion milling to a thickness appropriate for observation. A TEM (JEOL, JEM-2100F) with point to point resolution of 0.19 nm was used to observe the cross-sectional views with the electron acceleration voltage of 200 kV. Specimens of plan view observation were prepared by slightly scratching the film surface with a diamond pencil and transferring the films onto a copper microgrid. Then, the edges of the flakes produced by scratching were observed with the high resolution TEM (Thermo

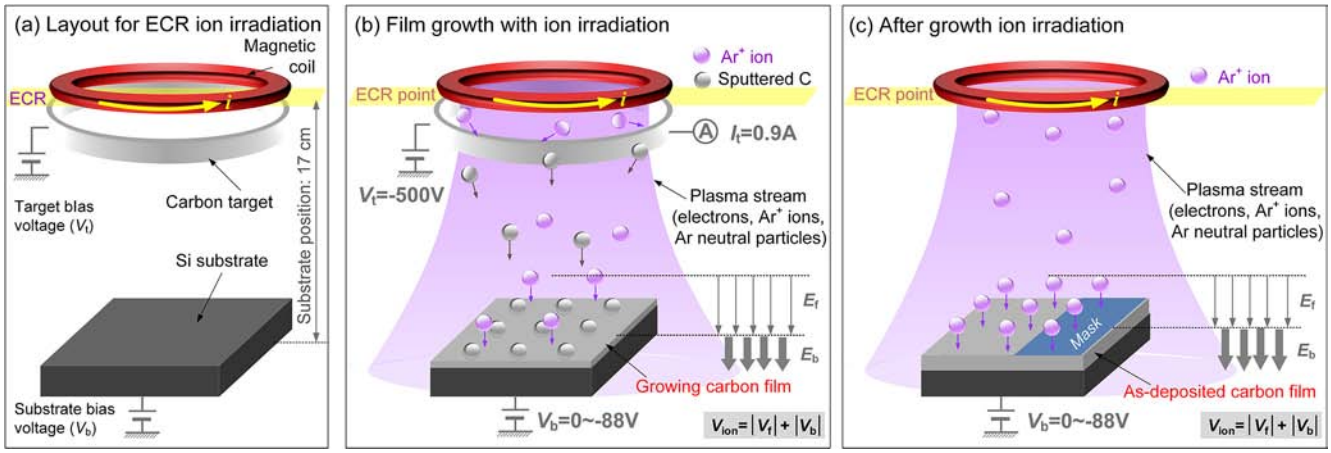

Fig. 1. Schematic illustrations of the experimental design for the low energy ion irradiation during and after film growth. (a) The layout of the core components in the ECR plasma sputtering system for low energy ion irradiation, (b) ion irradiation process during film growth on silicon substrate, (c) ion irradiation process after film growth on as-deposited carbon film with V_{ion} of 12 V.

Fisher Titan Themis G2). The TEM was operated at 80 kV with monochromator and image corrector, and the point to point resolution is 0.08 nm in TEM mode. The EELS signal was acquired in TEM mode with exposure time of 0.8 s overlapped with 5 frames for the carbon K edge. The core-loss spectra of carbon were obtained after subtracting a power-law background fit, and the spectra were executed a dark correction to remove the potentially effect from the camera. The X-ray photoelectron spectroscopy (XPS, Kratos, AXIS Ultra DLD) was used to analyze the bonding structures of sp^2 and sp^3 hybridizations. XPS spectra were obtained with a monochromatized Al Kα X-ray source (1486.6 eV) and a neutralizer. In order to further analyze the nanocrystallite structure in the films, Raman spectra were used, which was obtained by using a Raman spectrometer (Raman, HORIBA, LabRAM HR800). In this study, the 514 nm laser spot size was focused to 2 μm using a 100× objective, and the laser power was kept at 0.1 mW to avoid sample surface heating. Raman spectra between 1100 and 2000 cm^{-1} were acquired and analyzed.

2.3. Surface properties tests

The surface morphology of the carbon films was measured by atomic force microscope (AFM, BRUKER, Innova) under tipping mode. Silicon tip with curvature radius of 4 nm was used, and the images were obtained with scan size of 1 μm × 1 μm, scan frequency of 0.75 Hz and loading force of 2–4 μN. Five different positions were chosen to test the surface uniformity. To evaluate the top-surface scratch resistance, a three-sided pyramidal diamond tip with nominal tip radius of 80 nm was used to scratch the film surface and the loading force was 40 μN. After the nanoscratch test, the scratch depth was acquired by scanning the section profiles of the scratch track. In order to increase the reproducibility and accuracy of the measurements, we performed the double check measurement. Reference carbon films were measured before and after the intended measurement. The correction rate was less than 10% to the total measurements. To study the nanoscale adhesive behavior of carbon films, an AFM silicon tip with curvature radius of 4 nm was used to contact with the film top surface, and force-displacement curves were obtained during the approaching and retraction processes. The cantilever stiffness of the tip was 0.04 N/m, and the loading force was 10 nN. Five repeated tests were performed on each sample, and the standard deviation error was given.

3. Results and discussions

3.1. Low energy ion irradiation effects

The ion irradiation effects were studied by performing ion irradiation on the as-deposited carbon films with V_{ion} of 12 V. As shown from the inset in Fig. 2, the top surface of the as-deposited film was partially covered to protect the original surface. Then, the mask was removed after irradiation and the irradiation depth was tested by the steps. With different ion accelerating voltages, the etching rate was measured by dividing the irradiation depth with time, and the results were shown in Fig. 2. With V_{ion}s of 12 V, 20 V and 35 V, there is no irradiation depth can be measured, and the etching rate is zero. With V_{ion}s of 40 V, 50 V, 60 V, 75 V, 90 V and 100 V, the etching rate gradually increased with the increasing of ion irradiation energy. The linear fitting line in Fig. 2 showed that etching actually occurred and there existed a threshold voltage for physical etching at around 35 V for the low energy ion irradiation in ECR plasma. When the irradiation effects are considered in carbon nanostructure growth, the effects can be divided into the one that displaces the atoms, and the others that induce heating, electronic exciting and some other excitation affects that no primary damage is caused. Therefore, according to the etching rate measured in Fig. 2, the low energy ion irradiation in ECR plasma affected the carbon nanostructure growth in two ways: before the threshold voltage for physical etching, the film growth was induced by ion excitation effect, and after the threshold voltage, the film growth was induced by ion etching effect.

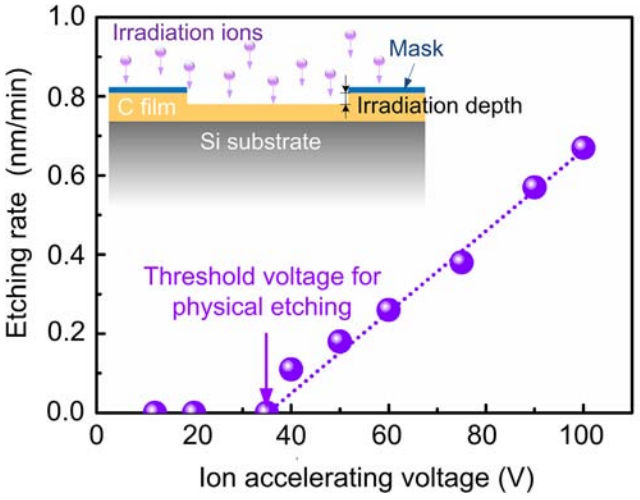

Fig. 2. Etching rate of the low energy ion irradiation. Insert figure shows the method to test the etching rate: carbon film was partially covered by a mask, then pure ion irradiation was performed, and the etching rate was calculated by dividing the irradiation depth with time.

In this paper, we prepared carbon films with different ion accelerating voltages, which involved in both the ion excitation and ion etching effects. We attributed the structural evolution to the ion irradiation induced effects during film growth, since the films were prepared very thin (40 nm) to control the temperature increase to less than 50 °C, which is much lower than the temperature for surface diffusion and graphitic thermal atomic rearrangement [30]. The growth mechanisms of carbon films under ion excitation and ion etching effects were shown in Fig. 3. With the ion excitation effect, the incident ions did not bring enough energy to move the carbon atoms. However, the electronic excitations during collisions activated the electrons of the covalent bonded top-most carbon atoms, which may result in a bond breaking, once one excited carbon atom encountered another excited carbon atom nearby, the thermodynamically stable sp^2 bonded structure is formed, as shown in Fig. 3(a)-A. Since the protruding regions of the growing surface will receive more depositing species and incoming ions than those located at lower heights [31], the sp^2 dominant nanocrystallite can grow faster along the vertical direction, as the schematic shown in Fig. 3(a)-B. Fig. 3(a)-C gave the actual cross-sectional TEM image of the film prepared with V_{ion} of 12 V, the vertically aligned nanostructure verified the schematic growth models. When the physical etching effect worked with V_{ion}s of 50–100 V, the irradiated ions broke the weak bonds between carbon atoms. Then the carbon atoms can move to another place to form new bonds, and much more cross-linking bonds between different graphene layers generated [32,33], as shown in Fig. 3(b)-A. As a result, the length of graphene layer was shortened by cross-linkings, as shown in Fig. 3(b)-B. Fig. 3(b)-C shows the actual cross-sectional TEM image of the film prepared with V_{ion} of 75 V to prove the grow mechanism under ion etching effect. According to the different film growth mechanisms with ion excitation and ion etching, obviously different nanostructures can be expected.

3.2. Nanostructural evolution

The nanostructures of the low energy ion irradiated carbon films were observed by high resolution TEM, and the results were shown in Fig. 4. Fig. 4(a) exhibited the cross-sectional view of the carbon film prepared with V_{ion} of 12 V, the middle part is the film with thickness of 40 nm, and sp^2 dominant nanocrystallites grown vertically aligned to the substrate can be found. Fig. 4(b) is the plan view for the film with

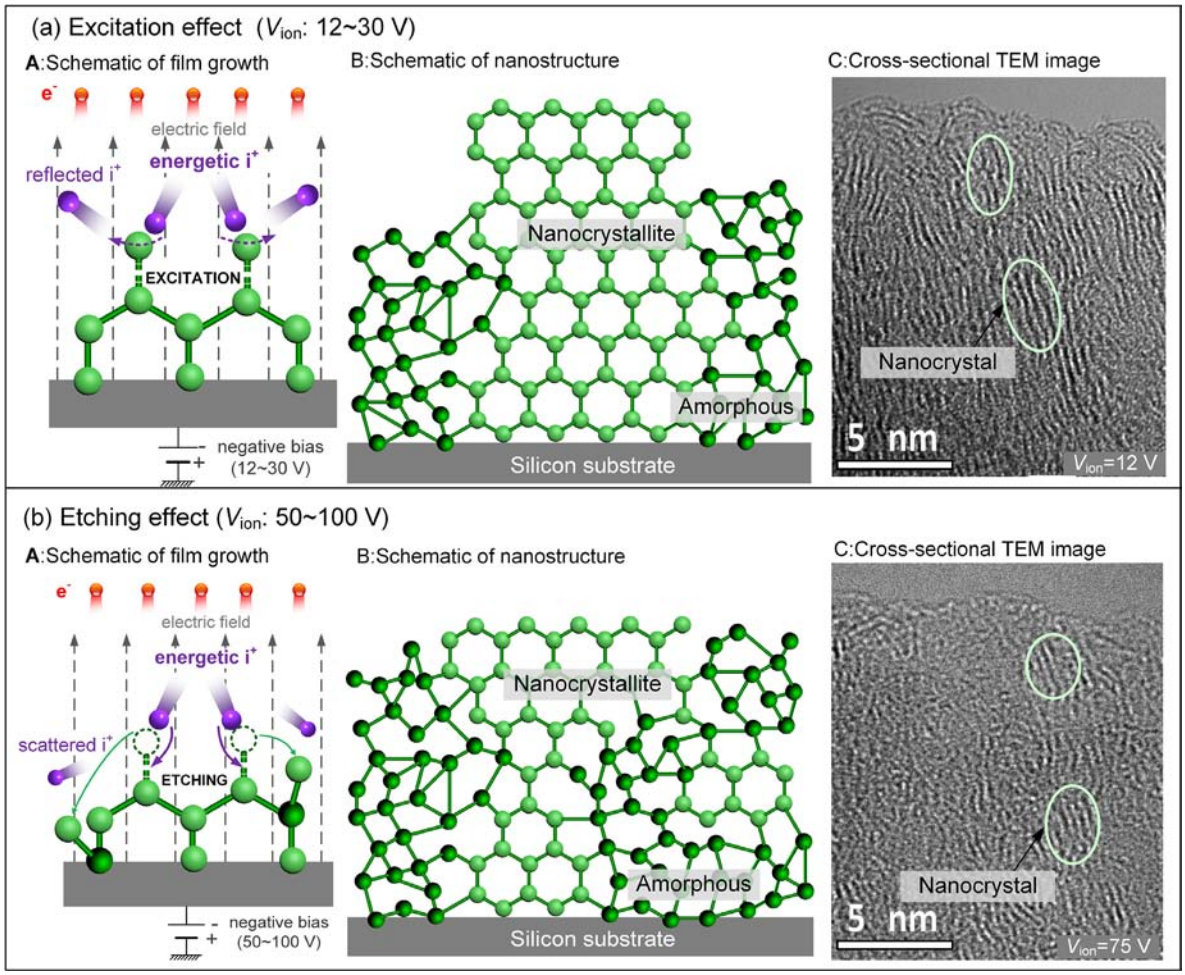

Fig. 3. Growth mechanism of the carbon films with ion excitation effect (a) and ion etching effect (b). A show the interactions between ions and carbon atoms under ion excitation and ion etching effect, B show the schematics for the carbon nanostructures with two different ion irradiation effects, C show the representative cross-sectional TEM images for ion excitation and ion etching, respectively.

V_{ion} of 12 V, the film consisted of sp^2 dominant nanocrystallites as marked in the image. Within the structure, the sp^2 bonded layers with interlayer space of 0.34 nm existed in the domains, at the edge, the parallel basal planes were cross-linked with each other by waving and twisting. The fast Fourier transformation (FFT) results on the upper-right corner shows white rings, indicating the existence of ordered nanostructure in the films. The core-loss EELS spectrum was shown in the lower-right corner, a π* peak around 285 eV appears, indicating the presence of sp^2 bonded carbon atoms, and a peak at 292 eV of σ* band reveals the presence of crystalline structure in carbon films [34,35]. Fig. 4(c) showed the other film grown with ion excitation effect (V_{ion} of 30 V), there are also sp^2 dominant nanocrystallites in the film, and the size was comparable to that in Fig. 4(b). Fig. 4(d)–(f) showed the nanostructures of the carbon films prepared with ion etching effect, in which the nanostructures were trending towards amorphous, and only very small sp^2 nanocrystallites domains can be found. The carbon films consisted of more disordered cross-linking nanostructure and the FFT images exhibited the characteristics of amorphous structure. Moreover, considering the π* and σ* peak ratio, the values for ion excited carbon films are higher than those for ion etched films, marking the presence of sp^2 nanocrystallites in the films is different with the two ion irradiation effects. The TEM and EELS results indicated that the nanostructure of sp^2 dominant nanocrystallited carbon films had two different characteristics with ion excitation and ion etching effect, respectively.

In order to further examine the structural evolution of the sp^2 dominant nanocrystallited carbon films with low energy ion irradiation systematically, XPS and Raman were used to determine the nature of bonding status in the carbon films with different ion irradiation effects, and the results were shown in Fig. 5. The sp^2 and sp^3 hybridization components were quantitatively obtained by deconvoluting the original C1s spectrum into three Gaussian-Lorentzian distribution curves, as shown from the inset in Fig. 5(a). Except for the sp^2 and sp^3 peaks, a small C-O peak was fitted, which is due to the surface contaminants, and the results showed equivalence of relative changes within a sample set. The evolution of sp^2/sp^3 was shown in Fig. 5(a). The carbon films prepared with ion excitation effect contained twice sp^2 hybridization than the sp^3 one. Then, there is a sharp transition between V_{ion} of 30–50 V, in which lay in the threshold voltage for physical etching. For the films prepared with ion etching effect, the sp^3 hybridization increased in the films, and the value of sp^2/sp^3 decreased to about 1.2, which means that more sp^2 hybridizations transferred to the sp^3 ones with the etching effect. To analyze the sp^2 dominant nanocrystallites, Raman spectra of the carbon films were measured, from which the mean nanocrystallite size can be quantitatively analyzed. As shown from the inset in Fig. 5(b), the original spectrum was fitted to the *D* band and the *G* band with a Lorentzian peak and a Breit-Fano-Wagner (BFW) peak, respectively. From the fitting curves, the intensity ratio of *D* to *G* bands (I_D/I_G) was obtained, which is normally proportional to the clustering of rings. And the mean nanocrystallite size (*L*) in the carbon films could be calculated by the following function [36]:

$$\frac{I_D}{I_G} = C(\lambda)L^2 \quad (1)$$

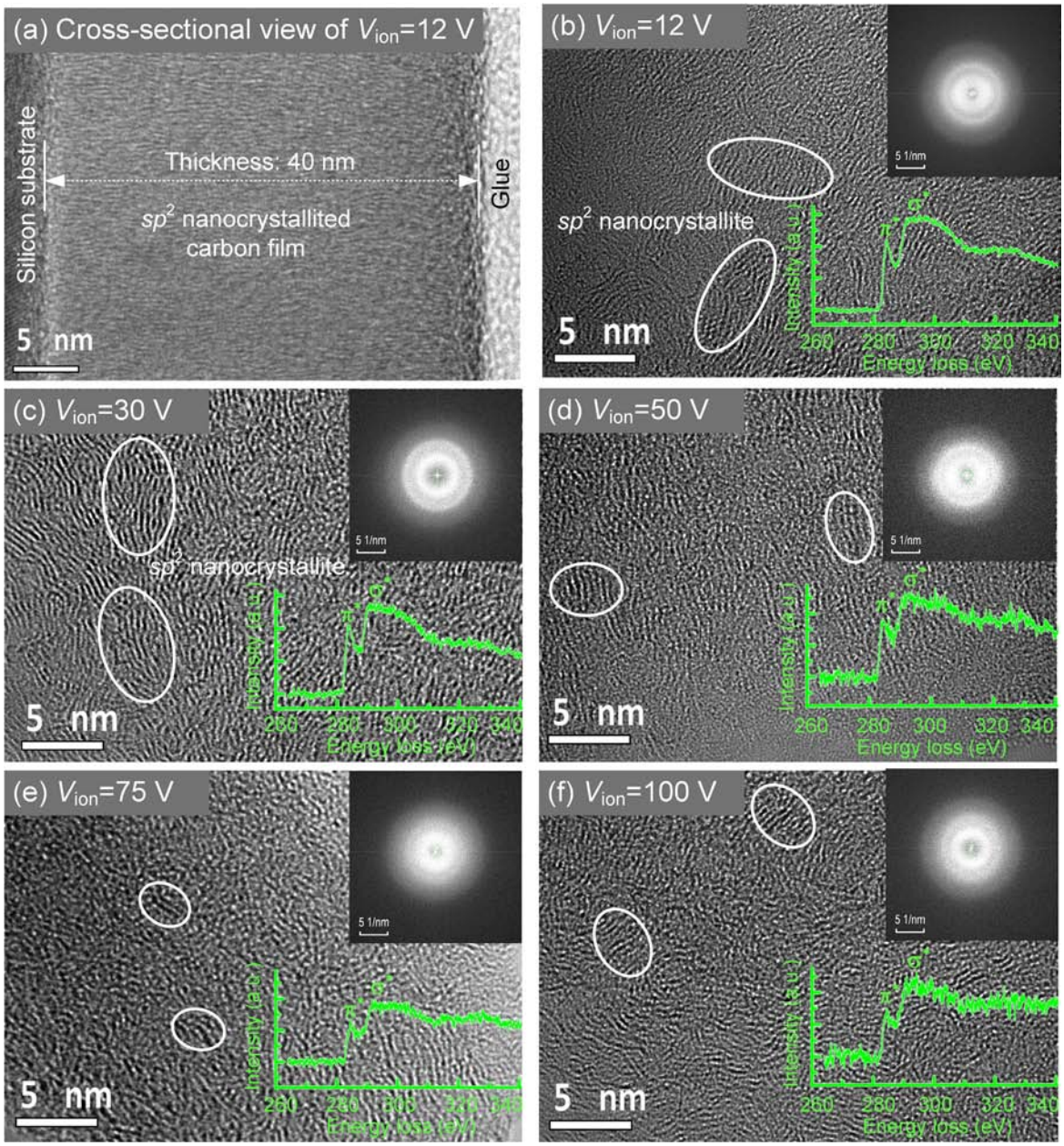

Fig. 4. Nanostructure of the low energy ion irradiated carbon films observed by TEM. (a) the cross-sectional view TEM images of carbon film prepared with V_{ion} of 12 V. (b) to (f) are the plan views for the films prepared with V_{ion} of 12 V, 30 V, 50 V, 75 V and 100 V respectively, the inserted FFT images and core-loss EELS spectra indicating the existence of sp^2 dominant nanocrystallites.

where C(λ) is a constant depends on the laser wavelength used for Raman spectrum excitation, which is 0.0055 when 541 nm laser is used.

The sp^2 nanocrystallite size showed different values for the carbon films prepared with different ion irradiation effects, as shown in Fig. 5(b). The nanocrystallite size was about 1.8–1.9 nm with ion excitation effect and decreased to 1.5–1.6 nm with ion etching effect. The nanostructure characterization results showed the same changing trends from the TEM images, sp^2/sp^3 value, and the nanocrystallite size, just as the predicted results shown in Fig. 3. With the ion excitation effect, sp^2 dominant nanocrystallited carbon films with larger nanocrystal size were obtained; with the ion etching effect, the nanocrystal size decreased and the sp^3 hybridization increased correspondingly.

3.3. Top-surface roughness

The surface morphologies of the carbon films were scanned by using the AFM, and the surface root-mean-square (RMS) roughness, R_q was obtained. Fig. 6(a) shows the surface morphological image of the carbon film prepared with ion excitation effect (V_{ion} of 12 V), small domes and peaks uniformly distributed on the surface, and R_q was 0.112 nm. Fig. 6(b) and (c) show the surface morphologies of the carbon films prepared with ion etching effect (V_{ion}s of 50 V and 75 V). With the same scale bar to Fig. 6(a), the surfaces were much platter, no obvious sharp peaks were observed on the surface, and the surface roughness was only about a half of the ion excited carbon films. Fig. 6(d) shows the summarized surface roughness with different V_{ion}s. The surface roughness also exhibited a suddenly decrease from 0.11 nm to about 0.05 nm when the V_{ion} increased from 30 V to 50 V. For the carbon films grown with ion excitation effect, the growth rate along the vertical direction was faster since the excited atoms on the top preferentially received more exciting particles and bonding atoms. On the contrary, for the films grown with ion etching effect, the weakly bonded

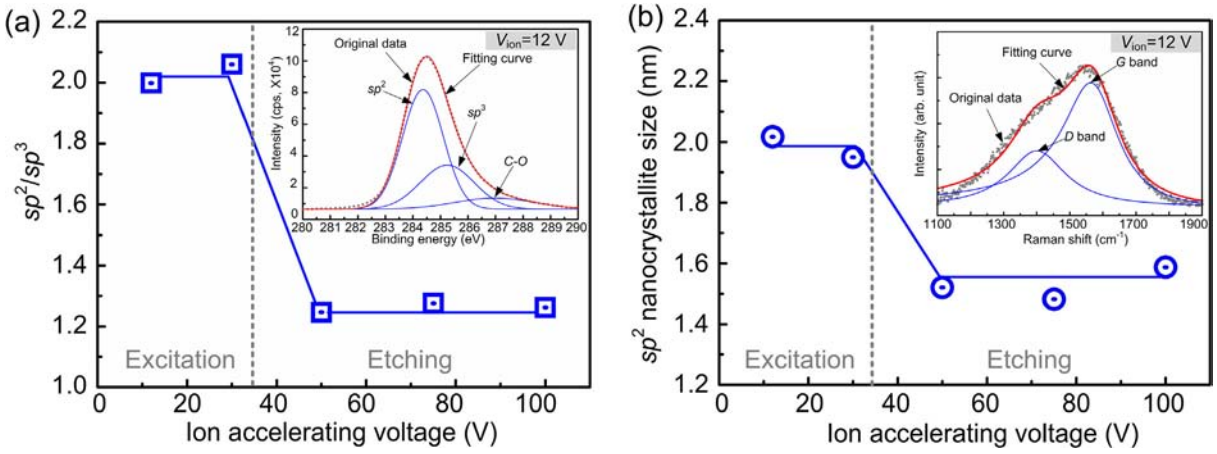

Fig. 5. The structural evolution of the low energy ion irradiated carbon films. (a) The sp^2/sp^3 value of the carbon films with different ion accelerating voltages, inset figure showed the representative fitting curves with sp^2, sp^3 and C-O peaks. (b) The sp^2 dominant nanocrystallite size of the carbon films with different ion accelerating voltages, inset figure showed the representative fitting curves with *D* band and *G* band.

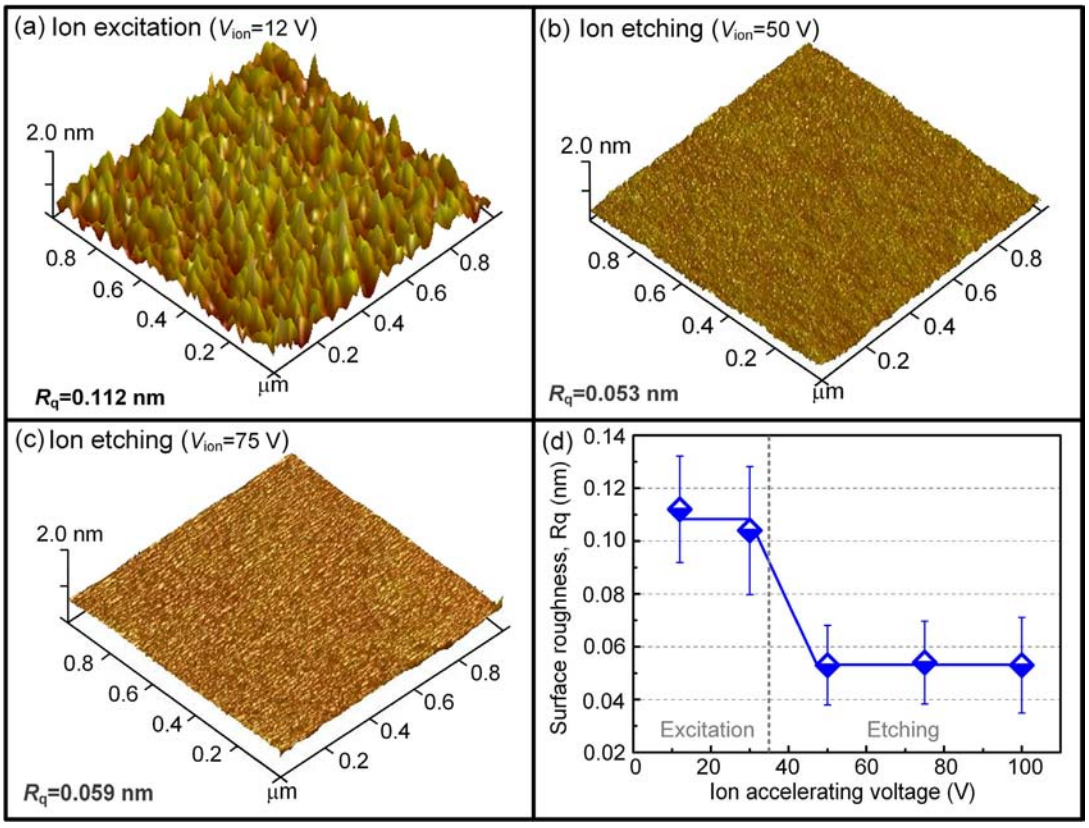

Fig. 6. (a) The surface morphology of ion excited carbon film with V_{ion} of 12 V with RMS roughness of 0.112 nm, (b) and (c) The surface morphologies of ion etched carbon film with RMS roughness of 0.053 nm and 0.059 nm with V_{ion} of 50 V and 75 V, respectively, (d) Surface roughness of the carbon films with different ion accelerating voltages.

carbon atoms would be sputtered to another place with etching ions. Then, the quick growth along the vertical direction was inhibited and the growth rate along the horizontal direction was increased. As a result, the films grown with ion excitation had rougher surface, while those with ion etching effect exhibited very smooth surfaces.

3.4. Top-surface nanoscratch

The nanoscratch behavior of the low energy ion irradiated carbon films was studied with the nanoscratch depth. The nanoscratch depth was obtained by scanning the wear tracks and made sectional lines across the wear tracks, as shown from the inset in Fig. 7. Fig. 7 shows the nanoscratch depth of the sp^2 dominant nanocrystallited carbon films with different ion accelerating voltages. The nanoscratch depths kept around 2.6 nm for the films grown with ion excitation, whereas the depths clearly decrease to about 0.5 nm when ion etching effect worked. The scratch test on diamond gave a scratch depth of 0.5 nm [37], and the nanocrystallited carbon films grown with ion etching effect showed an ultrahigh scratch resistance comparable to that of diamond. Based on the results, we know that when V_{ion} exceeds the threshold voltage, physical etching occurs, the cross-linkings and the sp^3 hybridizations in the films were increased. As a result, the films

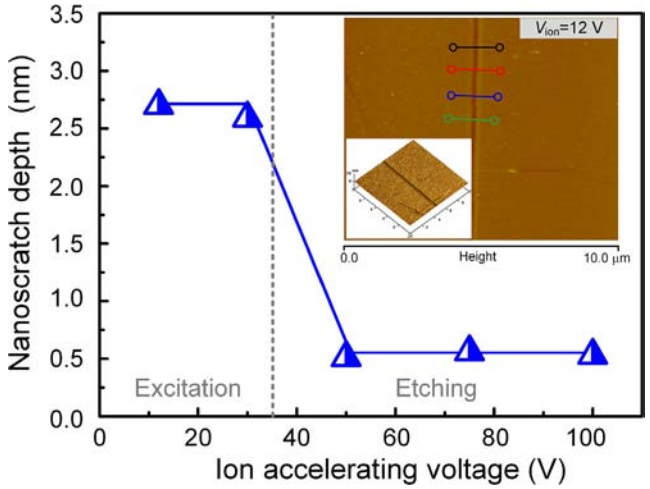

Fig. 7. The nanoscratch behavior of sp^2 dominant nanocrystallited carbon films, insert figure shows the AFM scanning image of nanoscratch track, and the cross-track sectional lines, by which the scratch depth can be accurately obtained.

grown harder, resulting in a much smaller nanoscratch depth.

3.5. Top-surface adhesion

The surface adhesive property was evaluated by the AFM, and adhesive force can be extracted from the tip snap off point, as shown from the inset in Fig. 8. In our measurements, areas which did not contain any large hillocks were selected, since such hillocks would lead to scatter in the adhesive force data. The adhesive forces of the sp^2 dominant nanocrystallited carbon films with different ion accelerating voltages were summarized in Fig. 8. Similar to the surface roughness and nanoscratch depth, the adhesive forces of the ion excited carbon films were relative high and those of the ion etched carbon films were decreased to about 7.5 nN. It is known that the adhesive force extracted from the pull-off curve is strongly affected by the surface roughness, and the force is usually increased with the decreasing of surface roughness [26]. However, in this study, the adhesive force decreased with the decreasing of roughness, and we ascribed this phenomenon to the nanostructure effect. With the ion etching effect, the carbon film had smaller nanocrystallite size with more cross-linkings and sp^3 hybridizations, which increased the hardness of the films, as shown in Fig. 7. The nanostructure finally led to a decreasing of contact area

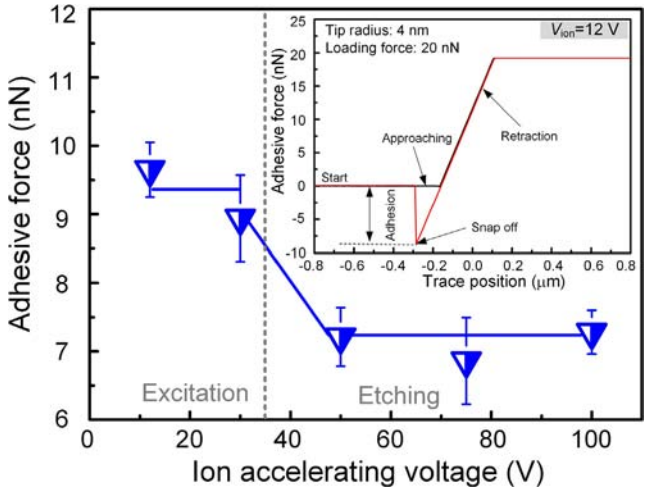

Fig. 8. The nanosurface adhesive behavior of sp^2 dominant nanocrystallited carbon films, insert figure shows the force-displacement curve during the approaching and retraction processes.

during the adhesion test, and the adhesive force for the ion etched carbon films decreased correspondingly.

3.6. Carbon films with after growth ion irradiation

In the above study, we found ion excitation and ion etching effects during the film growth. After film growth, how did the two effects affect the sp^2 nanocrystallite structure and the top-surface properties were further explored, and the results were shown in Fig. 9. The after growth ion irradiations were performed on the as-deposited sp^2 nanocrystallited carbon films and the blue dots in Fig. 9(c)–(f) showed the results of original film. With the after growth ion irradiation, the incident ions can only affect the topmost few nanometer thick layer [38]. Therefore, the main structure was nearly the same with the as-deposited film, as shown in Fig. 9(a) and (b). The sp^2 dominant nanocrystallite size was barely changed no matter the surface was affected by the ion excitation or the ion etching effects. Owing to the shallower XPS measurement depth of a few nanometers, the value of sp^2/sp^3 can reflect the changes of chemical bonding configuration in the topmost layer, which linearly decreased from 1.8 to 1.4 with the increasing of ion accelerating voltage. The surface roughness was obviously decreased when ion etching effect worked, which confirmed that the etching effect can break the weak bonds and move away the domed carbon atoms. One thing should be noticed that R_q gradually decreased until V_{ion} is higher than 50 V. The ion induced surface smoothing increased with the ion energy until subplantation effects at deeper lengths start to operate [39], which resulted that the surface roughness saturated at the minimum attained value and it was not further reduced for higher ion accelerating voltage. For the after growth irradiations, the topmost surface was irradiated, where the sp^3 hybridizations increased with the ion etching effect. As a result, the after growth irradiation with ion excitation effect did not affect the scratch depth, while the ion etching effect only can slightly decrease the scratch depth to about 1.8 nm. Finally, for the carbon films with after growth ion irradiation, the nanostructure effect disappeared, and the adhesive force is highly sensitive to the surface roughness, which resulted in the increasing of adhesive force with the decreasing of surface roughness. The results of after growth ion irradiation further confirmed the ion excitation and ion etching effects on the nanostructure and the top-surface properties of sp^2 dominant nanocrystallited carbon films.

4. Conclusions

In summary, we presented the low energy ion irradiation effects in electron cyclotron resonance (ECR) plasma on the formation and the top-surface properties of sp^2 nanocrystallited carbon films. The ion irradiation effects within ion accelerating voltage from 12 V to 100 V were divided into ion excitation and ion etching identified by the ion etching rate. A threshold voltage for physical etching was found to be about 35 V, which separated the two ion irradiation effects. Below the threshold voltage, the films growth was induced by ion excitation effect. The ions excited the electrons of the covalent bonded carbon atoms, and the electronic excitation promoted the growth of sp^2 nanocrystallite, as a result, the nanocrystallite size in the film was large. When the ion energy exceeded the threshold voltage, the films growth was induced by ion etching effect. The ions brought enough energy to break the bond and inhibit the growth of sp^2 nanocrystallite, which resulting in small nanocrystallite size. The top-surface properties of sp^2 nanocrystallited carbon films prepared with different ion irradiation effects showed different results. The ion etched carbon films had smaller surface roughness, nanoscratch depth and adhesive force compared with the ion excited carbon films. The after growth ion irradiation on the as-deposited carbon film further verified the ion excitation and ion etching effects on the nanostructure and the top-surface properties of sp^2 nanocrystallited carbon films. These findings shed light on the fabrication and applications of carbon based nanostructured

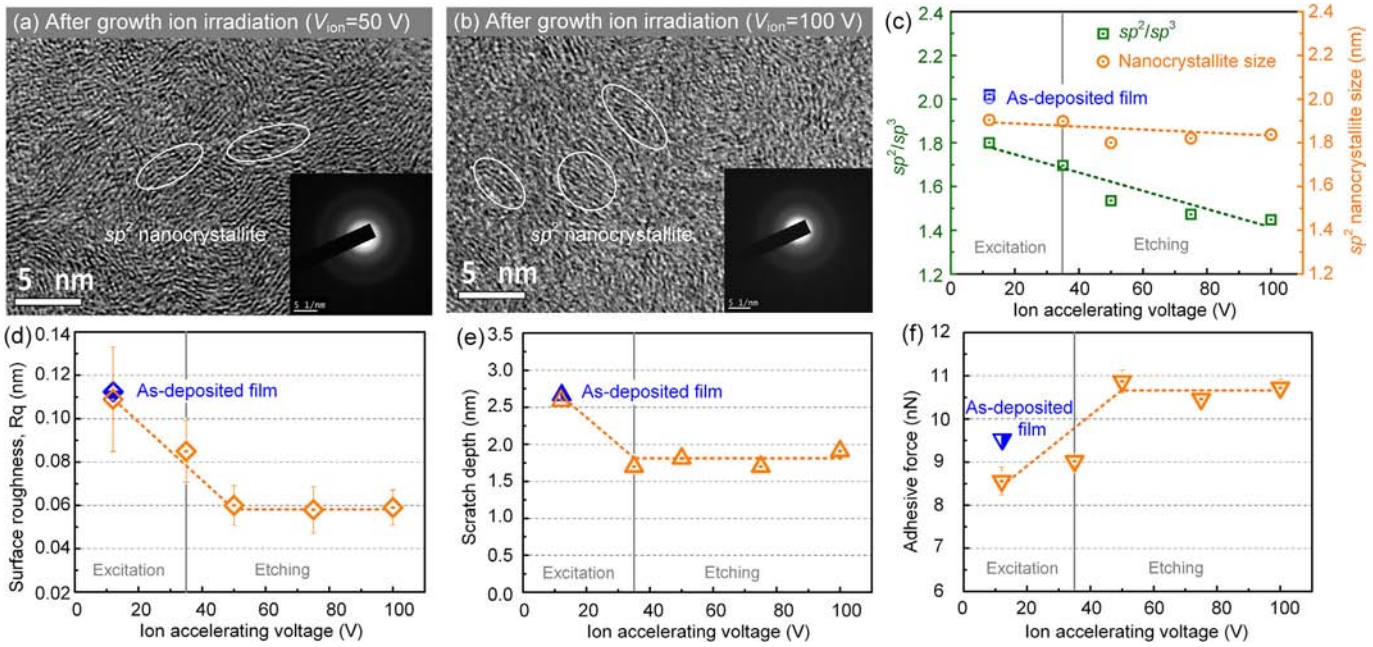

Fig. 9. The nanostructure and top-surface properties of the carbon films with after growth ion irradiation. (a) and (b) show that the sp^2 nanocrystallite in the film barely changed with ion etching effect from the TEM images, (c) shows the nanostructure evolution with different ion irradiation effects, (d)–(f) show the top-surface properties of roughness, nanoscratch depth and adhesive force, respectively. (The blue signs in Figs. (b)–(f) represent the results of as-deposited carbon film without after growth ion irradiation). (For interpretation of the references to colour in this figure legend, the reader is referred to the web version of this article.)

materials.

Acknowledgement

The Electron Microscope Center (EMC) of Shenzhen University is kindly acknowledged for instrument time and technical support. The authors also would like to thank the supports from the National Nature Science Foundation of China (Grant Nos.: 51305332 and 51575359), and Shenzhen Fundamental Research projects (Grant Nos.: JCYJ20170817100822005 and JCYJ20160427105015701).

References

[1] X. Fan, K. Nose, D.F. Diao, T. Yoshida, Nanoindentation behaviors of amorphous carbon films containing nanocrystalline graphite and diamond clusters prepared by radio frequency sputtering, Appl. Surf. Sci. 273 (2013) 816–823.
[2] E.H.T. Teo, A. Bolker, R. Kalish, C. Saguy, Nano-patterning of through-film conductivity in anisotropic amorphous carbon induced using conductive atomic force microscopy, Carbon 49 (2011) 2679–2682.
[3] C. Wang, D.F. Diao, Self-magnetism induced large magnetoresistance at room temperature region in graphene nanocrystallited carbon film, Carbon 112 (2017) 162–168.
[4] L. Yang, G.J. Hu, D.Q. Zhang, D.F. Diao, Nanosized graphene sheets enhanced photoelectric behavior of carbon film on psilicon substrate, Appl. Phys. Lett. 109 (2016) 031910.
[5] A.V. Krasheninnikov, K. Nordlund, Ion and electron irradiation-induced effects in nanostructured materials, J. Appl. Phys. 107 (2010) 071301.
[6] C. Wang, D.F. Diao, X. Fan, C. Chen, Graphene sheets embedded carbon film prepared by electron irradiation in electron cyclotron resonance plasma, Appl. Phys. Lett. 100 (2012) 231909.
[7] S. Talapatra, J.Y. Cheng, N. Chakrapani, S. Trasobares, A. Cao, R. Vajtai, M.B. Huang, P.M. Ajayan, Ion irradiation induced structural modifications in diamond nanoparticles, Nanotechnology 17 (2006) 305–309.
[8] D.W.M. Lau, A. Moafi, M.B. Taylor, J.G. Partridge, D.G. McCulloch, R.C. Powles, D.R. McKenzie, The structural phases of non-crystalline carbon prepared by physical vapor deposition, Carbon 47 (2009) 3263–3270.
[9] W.C. Chen, X. Zhang, D.F. Diao, Low-energy electron excitation effect on formation of graphene nanocrystallites during carbon film growth process, Appl. Phys. Lett. 111 (2017) 114105.
[10] W.L. Zhang, D.F. Diao, Three-layered sandwich structured carbon film prepared by ECR ion/electron/ion alternative irradiation technique, Surf. Coat. Technol. 278 (2015) 12–17.
[11] A.V. Krasheninnikov, F. Banhart, Engineering of nanostructured carbon materials with electron or ion beams, Nat. Mater. 6 (2007) 723–733.
[12] F. Banhart, Irradiation effects in carbon nanostructures, Rep. Prog. Phys. 62 (1999) 1181–1221.
[13] J. Robertson, Deposition mechanisms for promoting sp^3 bonding in diamond-like carbon, Diamond Relat. Mater. 2 (1993) 984–989.
[14] J.G. Buijnsters, M. Camero, L. Vázquez, Growth dynamics of ultrasmooth hydrogenated amorphous carbon films, Phys. Rev. B 74 (2006) 155417.
[15] D.F. Diao, C. Wang, X. Fan, Frictional behavior of nanostructured carbon films, Friction 1 (2013) 63–71.
[16] X. Fan, D.F. Diao, K. Wang, C. Wang, Multi-functional ECR plasma sputtering system for preparing amorphous carbon and Al-O-Si films, Surf. Coat. Technol. 206 (2011) 1963–1970.
[17] Y. Wang, H. Li, L. Ji, F. Zhao, X. Liu, Q. Kong, Y. Wang, W. Quan, H. Zhou, J. Chen, The effect of duty cycle on the microstructure and properties of graphite-like amorphous carbon films prepared by unbalanced magnetron sputtering, J. Phys. D: Appl. Phys. 43 (2010) 505401.
[18] F. Frost, R. Fechner, B. Ziberi, J. Völlner, D. Flamm, A. Schindler, Large area smoothing of surfaces by ion bombardment: fundamentals and applications, J. Phys. Condens. Matter. 21 (2009) 224026.
[19] M. Moseler, P. Gumbsch, C. Casiraghi, A.C. Ferrari, J. Robertson, The ultrasmoothness of diamond-like carbon surfaces, Science 309 (2005) 1545–1548.
[20] A. Erdemir, C. Donnet, Tribology of diamond-like carbon films: recent progress and future prospects, J. Phys. D: Appl. Phys. 39 (2006) R311–R327.
[21] L. Hultman, S. Stafsröm, Z. Czigány, J. Neidhardt, N. Hellgren, I.F. Brunell, K. Suenaga, Cross-linked nano-onions of carbon nitride in the solid phase: existence of a novel $C_{48}N_{12}$ aza-fullerene, Phys. Rev. Lett. 87 (2001) 225503.
[22] W. Guo, C.Z. Zhu, T.X. Yu, C.H. Woo, B. Zhang, Y.T. Dai, Formation of sp^3 bonding in nanoindented carbon nanotubes and graphite, Phys. Rev. Lett. 93 (2004) 245502.
[23] Y.Y. Zhang, C.M. Wang, Y. Cheng, Y. Xiang, Mechanical properties of bilayer graphene sheets coupled by sp^3 bonding, Carbon 49 (2011) 4511–4517.
[24] X. Fan, D.F. Diao, The adhesion behavior of carbon coating studied by re-indentation during in situ TEM nanoindentation, Appl. Surf. Sci. 362 (2016) 49–55.
[25] F.W. DelRio, B.M.P. De, J.A. Knapp, E.D. Reedy, P.J. Clews, M.L. Dunn, The role of van der Waals forces in adhesion of micromachined surfaces, Nat. Mater. 4 (2005) 629–634.
[26] T.D.B. Jacobs, K.E. Ryan, P.L. Keating, D.S. Grierson, J.A. Lefever, K.T. Turner, J.A. Harrison, R.W. Carpick, The effect of atomic-scale roughness on the adhesion of nanoscale asperities: a combined simulation and experimental investigation, Tribol. Lett. 50 (2013) 81–93.
[27] S.N. Ramakrishna, L.Y. Clasohm, A. Rao, N.D. Spencer, Controlling adhesion force by means of nanoscale surface roughness, Langmuir 27 (2011) 9972–9978.
[28] K.E. Ryan, P.L. Keating, T.D.B. Jacobs, D.S. Grierson, K.T. Turner, R.W. Carpick, J.A. Harrison, Simulated adhesion between realistic hydrocarbon materials: effects of composition, roughness, and contact point, Langmuir 30 (2014) 2028–2037.
[29] M. Matsuoka, K. Ono, Magnetic field gradient effects on ion energy for electron cyclotron resonance microwave plasma stream, J. Vac. Sci. Technol. A 6 (1988) 25–29.
[30] H. Li, T. Xu, C. Wang, J. Chen, H. Zhou, H. Liu, Annealing effect on the structure, mechanical and tribological properties of hydrogenated diamond-like carbon films,

Thin Solid Films 515 (2006) 2153–2160.
[31] C. Casiraghi, A.C. Ferrari, R. Ohr, A.J. Flewitt, D.P. Chu, J. Robertson, Dynamic roughening of tetrahedral amorphous carbon, Phys. Rev. Lett. 91 (2003) 226104.
[32] M.G. Fyta, I.N. Remediakis, P.C. Kelires, Energetics and stability of nanostructured amorphous carbon, Phys. Rev. B 67 (2003) 035423.
[33] S. Uhlmann, Th. Frauenheim, Y. Lifshitz, Molecular-dynamics study of the fundamental processes involved in subplantation of diamondlike carbon, Phys. Rev. Lett. 81 (1998) 641–644.
[34] D.A. Muller, Y. Tzou, R. Raj, J. Silcox, Mapping sp^2 and sp^3 states of carbon at sub-nanometre spatial resolution, Nature 366 (1993) 725–727.
[35] M. Shakerzadeh, E.H.T. Teo, A. Sorkin, M. Bosman, B.K. Tay, H. Su, Plasma density induced formation of nanocrystals in physical vapor deposited carbon films, Carbon 49 (2011) 1733–1744.
[36] A.C. Ferrari, J. Robertson, Resonant Raman spectroscopy of disordered, amorphous, and diamondlike carbon, Phys. Rev. B 64 (2001) 075414.
[37] S. Hirono, S. Umemura, M. Tomita, R. Kaneko, Superhard conductive carbon nanocrystallite films, Appl. Phys. Lett. 80 (2002) 425–427.
[38] M.L. Guo, D.F. Diao, L. Yang, X. Fan, Restructured graphene sheets embedded carbon film by oxygen plasma etching and its tribological properties, Appl. Surf. Sci. 357 (2015) 771–776.
[39] Y. Lifshitz, T. Köhler, T. Frauenheim, I. Guzmann, A. Hoffman, R.Q. Zhang, X.T. Zhou, S.T. Lee, The mechanism of diamond nucleation from energetic species, Science 297 (2002) 1531–1533.